Bifunctional Ru-Cluster-Decorated Co$_3$B—Co(OH)$_2$ Hybrid Catalyst Synergistically Promotes NaBH$_4$ Hydrolysis and Water Splitting

Huatong Li,[a] Zhengqi Liu,[a] Lixia Wang,[a] Man Guo,[a] Tayirjan Taylor Isimjan,*[b] and Xiulin Yang*[a]

Abstract: Developing a highly efficient bifunctional catalyst for hydrolysis of metal hydrides and spontaneous hydrogen evolution reaction (HER) is essential for substituting conventional fuels for H$_2$ production. Herein, Ru-cluster-modified Co$_3$B—Co(OH)$_2$ supported on nickel foam (Ru/Co$_3$B—Co-(OH)$_2$@NF) is constructed by electroless deposition, calcination and chemical reduction. The catalyst exhibits an excellent hydrogen generation rate (HGR) of 4989 mL min^{-1} g$_{catalyst}^{-1}$ and good reusability, superior to most previously reported catalysts. Besides, Ru/Co$_3$B—Co(OH)$_2$@NF displays a prominent hydrogen evolution reaction catalytic capability with a low overpotential of 153.0 mV at 100 mA cm^{-2} (50.5 mV at 10 mA cm^{-2}), a small Tafel slope of 40.0 mV dec^{-1} and long-term stability (100 h@10 mA cm^{-2}) in 1.0 M KOH. The excellent catalytic H$_2$ generation capacity benefits from the rapid charge transfer promoted by metallic Co$_3$B, the synergistic catalytic effect of Co$_3$B—Co(OH)$_2$ and Ru clusters, and the unique composite structure favorable for solute transport and gas emission.

Introduction

Hydrogen is an excellent energy carrier and a promising alternative to fossil fuels because of its high gravimetric energy density.[1] Among the numerous hydrogen production strategies, electrochemical water splitting has attracted much attention due to its efficient hydrogen production capacity.[2] However, the uphill reaction limits the application of electrochemical water splitting due to the high energy consumption and expensive cocatalysts.[3] The most advanced hydrogen evolution reaction (HER) catalysts are based on the costly noble metal platinum (Pt).[4] Even though extensive studies focused on non-noble metal catalysts, they still struggle with stability and high overpotentials.[5] Our early study proved that introducing small amounts of the cheapest noble metal, such as Ru, into the non-noble metal system would increase the catalytic performance and improve the catalyst stability and reusability.[6] Among all other transition metal sulphides, borides, phosphides, and oxides are widely investigated as promising electro-catalysts due to their variable compositions, tunable surface electronic configurations and good conductivity.[7] In addition, borides exhibit excellent electrocatalytic performance because of the unique electronic effect between transition metal atoms and boron atoms.[8] Besides, the oxides can accelerate the charge transfer rate via the synergistic effect between the heterostructures, thereby improving catalytic performance.[9] Depending upon previous report,[10] we selected transition metal boride as the base catalyst, which may also be a good candidate for metal hydride to tackle the hydrogen storage challenge. Low-cost hydrogen storage is another crucial step to realizing the hydrogen economy.[11] The typical strategies of hydrogen storage are used currently, either physical methods, high-pressure,[12] and using absorbents[13] or chemical storage through reversible chemical bonding.[14]

Along with the same line, hydrogen-containing compounds, including formic acid (HCOOH), lithium aluminum hydride (NaAlH$_4$), and sodium borohydride (NaBH$_4$) have received significant attention owing to their high H$_2$ content, chemical stability and nontoxicity.[15] Among them, NaBH$_4$ is the best candidate. Nevertheless, the self-hydrolysis of NaBH$_4$ is restricted by the sluggish reaction kinetics.[16] Ruthenium-based catalysts with excellent catalytic hydrolysis properties are considered perfect substitutes for Pt-based catalysts.[17] Meanwhile, both transition metal borides and oxides such as CoWB/NF,[18] Co—Mo—B/C,[19] Ir—Ru—B/CeO$_2$,[20] and Co$_3$O$_4$[21] also exhibit superior performance in NaBH$_4$ hydrolysis. Furthermore, the synergistic effect of heterostructures composed of different materials can significantly improve catalytic performance.[22]

In this work, we successfully fabricated Ru/Co$_3$B—Co(OH)$_2$ as bifunctional catalysts for both NaBH$_4$ hydrolysis and HER. Notably, the optimized catalyst exhibited excellent catalytic

[a] H. Li, Z. Liu, L. Wang, M. Guo, Prof. Dr. X. Yang
Guangxi Key Laboratory of Low Carbon Energy Materials
School of Chemistry and Pharmaceutical Sciences
Guangxi Normal University
541004 Guilin (P. R. China)
E-mail: xlyang@gxnu.edu.cn

[b] Dr. T. T. Isimjan
Saudi Arabia Basic Industries Corporation (SABIC) at
King Abdullah University of Science and Technology (KAUST)
23955-6900 Thuwal (Saudi Arabia)
E-mail: isimjant@sabic.com

🖥 *Supporting information for this article is available on the WWW under https://doi.org/10.1002/chem.202203207*

Chemistry–A European Journal

Research Article
doi.org/10.1002/chem.202203207

Chemistry Europe
European Chemical
Societies Publishing

activity in both cases. Moreover, Ru/Co₃B–Co(OH)₂ also showed superior reusability and long-term stability. X-ray diffraction (XRD) can confirm the existence of Co₃B and Co(OH)₂. The structure of Ru/Co₃B–Co(OH)₂, demonstrated by scanning electron microscopy (SEM), provided more active sites thereby improve the catalytic performance. X-ray photoelectron spectroscopy (XPS) can also corroborate the interaction between Ru clusters and Co₃B–Co(OH)₂ substrate.

Results and Discussion

The Ru/Co₃B–Co(OH)₂@NF composite was obtained in three consecutive steps (Figure 1a). Briefly, the b–Co₃B–Co(OH)₂ particles were firstly fabricated through the conventional deposition method. Secondly, the b–Co₃B–Co(OH)₂@NF was calcined at 350 °C in Ar atmosphere to acquire the Co₃B–Co-(OH)₂@NF. Finally, the Ru clusters were supported on the Co₃B–Co(OH)₂ (Ru/Co₃B–Co(OH)₂@NF) via sodium borohydride reduction method. XRD patterns elucidated the crystalline characteristics of the as-prepared catalysts. As illustrated in Figure 1b–c, the XRD pattern of b–Co₃B–Co(OH)₂, Co₃B–Co-(OH)₂, b–Ru/Co₃B–Co(OH)₂ and Ru/Co₃B–Co(OH)₂ are consistent with that of Co₃B (JCPDS: 12-0443) and Co(OH)₂ (JCPDS: 02-0925).[23] There was no significant change in the species before and after calcination. Additionally, the peak at around 69.4° is belonging to the (110) crystal plane of Ru.[24] The above results demonstrate that Ru/Co₃B–Co(OH)₂ is successfully fabricated.

The morphology of materials was characterized by SEM and transmission electron microscopy (TEM). The blank NF has a 3D structure with a smooth surface (Inset of Figure S1a). b–Ru/Co₃B–Co(OH)₂@NF and b–Co₃B–Co(OH)₂@NF exhibit an agglomerated particle structure (Figure 2a and Figures S1a–b). Although the components of the complexes were not significantly altered, the structure of materials changed after calcination, which increases the surface area of the catalyst and provides more reaction sites to facilitate the obtaining of well-dispersed Ru nanoclusters without severe agglomeration, thereby improving the catalytic activity (Figure 2b and Figures S1c–d).[25] As shown in Figure 2c, the Ru clusters with an average particle size of about 2.14 nm, which concluded from statistical results of about 200 Ru clusters, are uniformly dispersed on the Co₃B–Co(OH)₂ surface (red markers demonstrates the position of the Ru clusters). The high-resolution TEM image of Ru/Co₃B–Co(OH)₂@NF verifies the interplanar spacings of 0.20 and 0.14 nm, which correspond to the (022) and (110) lattice planes of Co₃B and Ru,[24] and the lattice spacing of 0.15 nm belongs to Co(OH)₂ species (Figure 2d). Besides, energy dispersive X-ray (EDX) pattern proves the coexistence of Co, B, Ru, O, and C elements (Figure S2). Atomic force microscopy (AFM) verifies the morphology of Ru/Co₃B–Co(OH)₂@NF with a thickness of about 10.5 nm (Figures 2e–f). Furthermore, the high-angle annular dark-field scanning transmission electron microscopy (HAADF-STEM) and corresponding energy-dispersive X-ray spectroscopy (EDS) mappings confirms the uniform dispersion of Ru, Co, B, and O on the surface of Ru/Co₃B–Co(OH)₂@NF (Figure 2g).
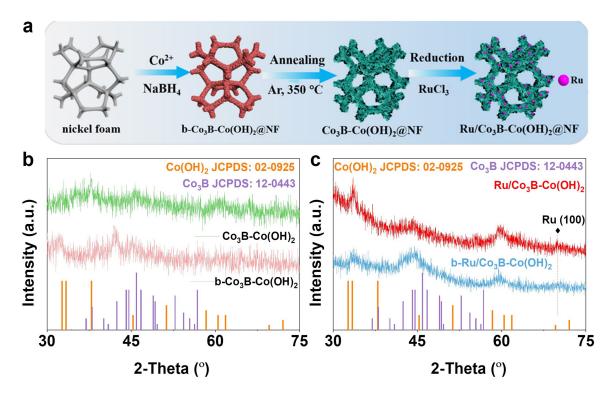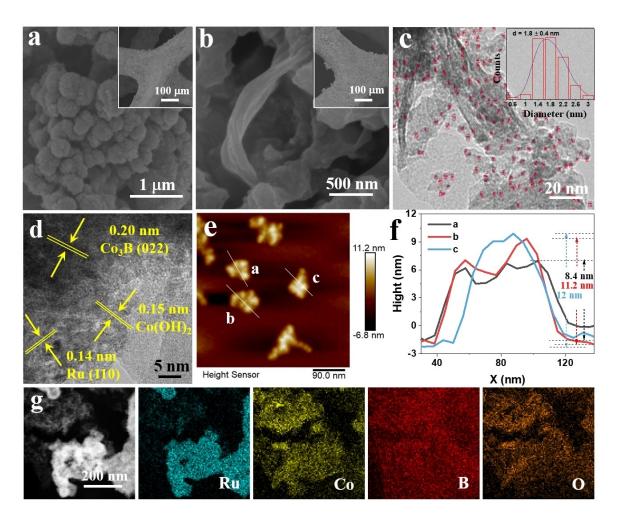

Figure 1. (a) Schematic diagram of the formation of Ru/Co₃B–Co(OH)₂@NF catalyst. XRD patterns of (b) Co₃B–Co(OH)₂ and b–Co₃B–Co(OH)₂, (c) Ru/Co₃B–Co(OH)₂ and b–Ru/Co₃B–Co(OH)₂ (Note: the test powder samples were scraped off the NF surface).

Chemistry–A European Journal

Research Article
doi.org/10.1002/chem.202203207

Chemistry
Europe
European Chemical
Societies Publishing

Figure 2. SEM images of (a) b–Ru/Co$_3$B–Co(OH)$_2$@NF, and (b) Ru/Co$_3$B–Co(OH)$_2$@NF. The insets are the low magnification SEM images. (c) TEM (Inset: a histogram of the particle size of distribution), (d) HR-TEM image of Ru/Co$_3$B–Co(OH)$_2$@NF, (e–f) AFM image and the corresponding height profiles, and (g) HAADF-STEM and EDS elemental mapping images of Ru/Co$_3$B–Co(OH)$_2$@NF.

XPS investigated the elemental composition and bonding states of materials. As shown in Figure S3a, the whole spectrum confirms the existence of Co, Ru, B, and O elements in Ru/Co$_3$B–Co(OH)$_2$@NF. In Figure 3a, the C 1s + Ru 3d spectra can be deconvoluted into three peaks at 284.8, 286.0, and 287.3 eV, which were indexed as C–C, C–O and C=O, respectively.[26] Additionally, the Ru 3$d_{5/2}$ spectra display two prominent peaks at 280.5 and 281.9 eV, assigning to metallic Ru^0 and oxidized Ru^{4+}.[27] The Ru content (45.6%) in Ru/Co$_3$B–Co(OH)$_2$@NF was approximately twice higher that of b–Ru/Co$_3$B–Co(OH)$_2$@NF (27.4%). Of note, due to the strong interaction between Ru precursors and the substrate, the calcination provides more porosity without aggregating Ru clusters. Moreover, the Ru species can be reduced quickly in sodium borohydride, which explains the high Ru^0 content in the Ru/Co$_3$B–Co(OH)$_2$ compared to that of b–Ru/Co$_3$B–Co(OH)$_2$.[25,28] The above results illustrate that the intrinsic activity of the catalyst can be improved by high-temperature treatment. Furthermore, the C 1s + Ru 3d spectra of other precursors were depicted in Figure S3b. As displayed in Figure 3b, the high-resolution Co 2p spectrum of Ru/Co$_3$B–Co(OH)$_2$@NF was fitted into three peaks:

Co–B (775.7 eV), Co–O (782.1 eV) and satellite (786.5 eV).[29] Compared to Co$_3$B–Co(OH)$_2$@NF, the binding energy of Co–O was positively shifted by 0.42 eV, which is caused by the electron transfer between Co(OH)$_2$ and Ru clusters. Moreover, the B 1s region of Ru/Co$_3$B–Co(OH)$_2$@NF was fitted to two peaks at 187.7 eV (Co–B) and 192.2 eV (B–O) (Figure 3c).[30] Meanwhile, the O 1s spectrum emerge three palpable peaks at 530.0, 531.3 and 532.6 eV can be attributed M–O, C–O and adsorbed H$_2$O, respectively. The metal-oxygen bond also corroborates the existence of Co(OH)$_2$ (Figure 3c).[31] More importantly, the high-resolution Co 2p and B 1s spectra of b–Co$_3$B–Co(OH)$_2$@NF were exhibited in Figure S3c–d, which possesses similar bonding states to Ru/Co$_3$B–Co(OH)$_2$@NF. Besides, the binding energy of b–Co$_3$B–Co(OH)$_2$@NF was not shifted relative to Co$_3$B–Co-(OH)$_2$@NF. The above results verify that the charge transfer in the composite occurs between Ru and Co(OH)$_2$, thereby accelerating the reaction kinetics.[32]

The catalytic hydrolysis of NaBH$_4$ for H$_2$ generation was carried out in an alkaline environment at 25 °C, wherein the generated H$_2$ gas was calculated by weighing the water mass-produced by the drainage method (Figure S4). Self-hydrolysis to
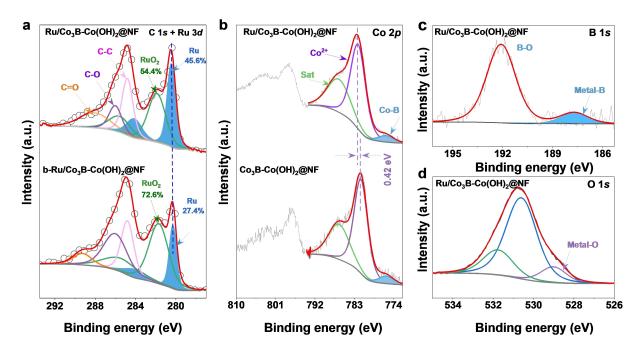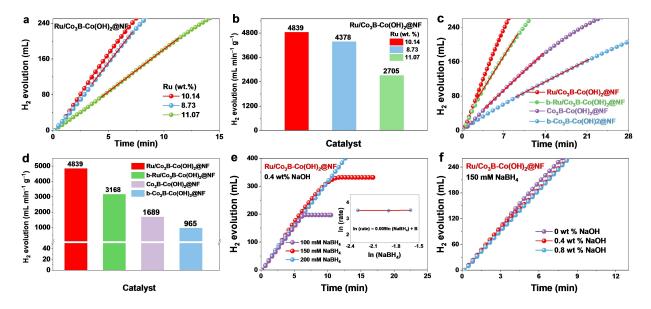
Chemistry–A European Journal

Research Article
doi.org/10.1002/chem.202203207

Chemistry
Europe
European Chemical
Societies Publishing

Figure 3. High-resolution XPS spectra of (a) C 1s + Ru 3d, (b) Co 2p, (c) B 1s and (d) O 1s regions of Ru/Co$_3$B–Co(OH)$_2$@NF, b–Ru/Co$_3$B–Co(OH)$_2$@NF and Co$_3$B–Co(OH)$_2$@NF.

produce 110 mL of hydrogen in 150 mM NaBH$_4$ solution takes about 10 h (Figure S5a), and only trace amounts of hydrogen gas are produced by hydrolysis of NaBH$_4$ at the same time with the presence of NaOH. The results indicate the critical role of NaOH as a stabilizer in the catalytic process (Figure S5b). Meanwhile, we explored the effect of Ru/Co$_3$B–Co(OH)$_2$@NF catalysts prepared by different Ru loadings on H$_2$ production by catalytic hydrolysis. The catalytic hydrolysis performance starts to increase drastically until the content is 10.1 wt.% and then decreases slightly with the increase of Ru loading. The optimal Ru content to achieve the highest activity could be due to the Ru aggregation and unique synergy between Ru and support. (Figure 4a).[27] The maximum catalytic hydrolysis HGR is 4839.0 mL min^{-1} g^{-1} (Figure 4b) when the content of Ru is 10.1 wt.%. Therefore, 10.1 wt.% Ru loading was kept during the rest of the optimization processes. The catalytic activity of Ru/

Figure 4. (a) Stoichiometric H$_2$ evolution in 150 mM NaBH$_4$ + 0.4 wt.% NaOH solution by Ru/Co$_3$B–Co(OH)$_2$@NF catalysts with different loadings of Ru at 25 °C, and (b) the corresponding HGR values. (c) H$_2$ evolution by different catalysts at 25 °C, and (d) the summarized HGR values. (e) The relationship between H$_2$ evolution and different NaBH$_4$ concentrations (Inset: the corresponding plot of ln (rate) vs ln (concentration of NaBH$_4$)) and (f) the relationship between H$_2$ evolution and different NaOH concentrations.
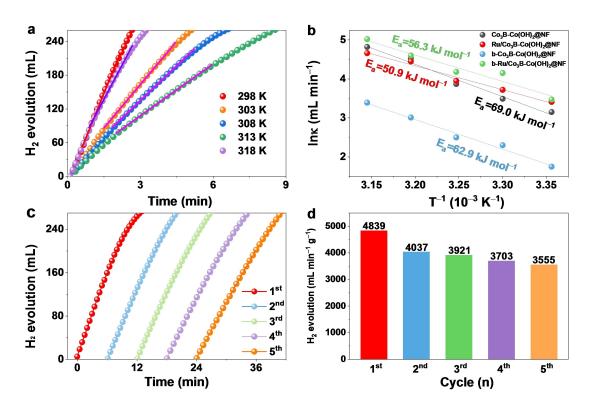
$Co_3B–Co(OH)_2@NF$ is significantly higher than that of all other control samples (Figure 4c). Meanwhile, the HGR of $Ru/Co_3B–Co(OH)_2@NF$ is approximately 1.53-, 2.87-, 5.01- and 11.39-fold higher than that of $b–Ru/Co_3B–Co(OH)_2@NF$, $Co_3B–Co(OH)_2@NF$, $b–Co_3B–Co(OH)_2@NF$ and $Ru/Co_3O_4@NF$, respectively (Figure 4d). Meanwhile, the high catalytic HGR is also superior to most of the previously reported catalysts (Table S2). There is no detectable correlation between sodium borohydride concentration and HGR (Figure 4e), indicating zero-order reaction kinetics (Inset of Figure 4e).[33] The NaOH has a minimum effect on the HGR as a stabilizing agent in borohydride hydrolysis. Thus, 0.4 wt.% NaOH concentration is selected in this work to align with the literature report (Figure 4f).[34] This result is different from Lu and coworkers,[35] who reported that the HGR from $NaBH_4$ solution was positively correlated with NaOH concentration within a specific concentration range, and the HGR would continuously decrease with further increasing NaOH concentration. Moreover, in our previous work, the HGR barely changed when NaOH concentration increased within a specific concentration.[27,34] Those results demonstrate that the effect of NaOH concentration on the $NaBH_4$ hydrolysis greatly depends on the catalyst's composition.[36]

The effect of temperature on the catalytic performance of $Ru/Co_3B–Co(OH)_2@NF$ and $Co_3B–Co(OH)_2@NF$ in alkalized $NaBH_4$ solution was further investigated. The results reveal that the catalytic performance increases with the increase of experimental temperature (Figure 5a and Figure S6). Moreover, the

activation energies of $Ru/Co_3B–Co(OH)_2@NF$ is estimated to be 50.9 kJ mol^{-1}, which is lower than that of $Co_3B–Co(OH)_2@NF$, $b–Ru/Co_3B–Co(OH)_2@NF$ and $b–Co_3B–Co(OH)_2@NF$ (Figure 5b), The result reveals a unique synergy between Ru and $Co_3B–Co(OH)_2$ support.[37] The reusability of the catalyst was evaluated by the continuous recycling experiments in alkalized $NaBH_4$ solution. The results show that the $Ru/Co_3B–Co(OH)_2@NF$ catalyst has an excellent recovery capacity for catalytic hydrogen production (Figure 5c). After the fifth cycle, the catalyst retained about 73.5% of its initial catalytic capacity, which is significantly better than those of $b–Ru/Co_3B–Co(OH)_2@NF$ (47.1%), $Co_3B–Co(OH)_2@NF$ (62.8%), and $b–Co_3B–Co(OH)_2@NF$ (67.1%) (Figure 5d, Figure S7). In addition, $Ru/Co_3B–Co(OH)_2@NF$ still basically maintains the original morphology, except that the surface is slightly damaged compared with the initial catalyst (Figure S10b). As can be seen from the XPS spectra, the proportion of Ru decreased slightly from 45.6% to 44.9% (the content of Ru species was reduced to 1.8 wt.% after five cycles (Table S1)) compared with before cyclic hydrolysis, which may be caused by the exfoliation of Ru and catalyst poisoning (Figure S11a).[38]

For bifunctional catalyst of $Ru/Co_3B–Co(OH)_2@NF$, the HER performance of the material was also measured in 1.0 M KOH solution. HER data were corrected to the RHE potential, and the calibration parameter was obtained in an H_2 saturated electrolyte (Figure S8). As presented in Figure 6a, $Ru/Co_3B–Co(OH)_2@NF$ exhibits excellent electrocatalytic performance with an overpotential of 153 mV to reach 100 mA cm^{-2}, slightly

Figure 5. (a) The relationship between the HGR and applied temperatures of $Ru/Co_3B–Co(OH)_2@NF$. (b) The summarized Arrhenius plots for $Ru/Co_3B–Co(OH)_2@NF$, $b–Ru/Co_3B–Co(OH)_2@NF$, $b–Co_3B–Co(OH)_2@NF$ and $Co_3B–Co(OH)_2@NF$. (c) Recycling stability test of $Ru/Co_3B–Co(OH)_2@NF$ catalyst in 150 mM $NaBH_4 + 0.4$ wt.% NaOH at 25 °C. (d) The summarized HGR values in the different recycling tests.

Chemistry–A European Journal

Research Article
doi.org/10.1002/chem.202203207

Chemistry Europe
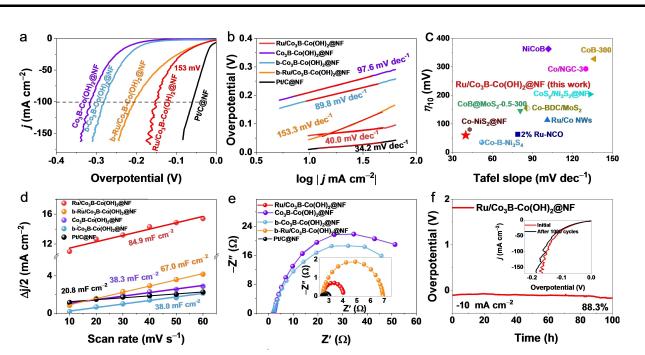European Chemical
Societies Publishing

Figure 6. (a) Polarization curves. (b) Tafel slopes. (c) Comparison of the HER performance of Ru/Co$_3$B–Co(OH)$_2$@NF with that of other recently reported catalysts. (d) Double-layer capacitance (C_{dl}) plots. (e) Electrochemical impedance spectroscopy (EIS) plots. (f) Durability test for Ru/Co$_3$B–Co(OH)$_2$@NF (Inset: Polarization curves before and after 1000 cycles).

inferior to Pt/C and far superior to b–Ru/Co$_3$B–Co(OH)$_2$@NF, b–Co$_3$B–Co(OH)$_2$@NF and Co$_3$B–Co(OH)$_2$@NF. The high fluctuation of LSV is due to the catalyst surface coverage by the access gas molecule at a higher current density, which could not leave the surface instantly. The Tafel slope indicates the fundamental and rate-determining steps during the HER process.[39] According to Figure 6b, the Tafel slope of Ru/Co$_3$B–Co(OH)$_2$@NF is 40.0 mV dec^{-1}, comparable to Pt/C@NF (34.2 mV dec^{-1}) and much lower than that of other samples, indicating that Ru/Co$_3$B–Co(OH)$_2$@NF possesses superior catalytic kinetics and follows the Volmer-Heyrovsky.[40] Additionally, the HER activity of Ru/Co$_3$B–Co(OH)$_2$@NF outperforms most recently reported catalysts (Figure 6c and Table S4). Since the surface area of the catalyst may affect the catalytic activity, the electrochemical activity-specific surface area was evaluated by the electrochemical double-layer capacitance (C_{dl}).[1a,41] In Figure 6d, the C_{dl} value of Ru/Co$_3$B–Co(OH)$_2$@NF is 84.9 mF cm^{-2}, higher than that of b–Ru/Co$_3$B–Co(OH)$_2$@NF (67.0 mF cm^{-2}), Co$_3$B–Co(OH)$_2$@NF (38.3 mF cm^{-2}), b–Co$_3$B–Co(OH)$_2$@NF (30.8 mF cm^{-2}) and Pt/C@NF (20.8 mF cm^{-2}), which manifests that the Ru/Co$_3$B–Co(OH)$_2$@NF has larger specific surface area.[42] Furthermore, electrochemical impedance spectroscopy (EIS) was performed to probe the interfacial properties and ascertain the electron transfer process.[43] The charge transfer resistance (R_{ct}) of Ru/Co$_3$B–Co(OH)$_2$@NF catalyst was slightly higher than that of Pt/C@NF but much lower than that of other electrodes, which indicates a faster electron-transfer (Figure 6e). The electrochemical stability of Ru/Co$_3$B–Co(OH)$_2$@NF catalyst was monitored by chronopotentiometry test (Figure 6f). The overpotential of Ru/Co$_3$B–Co(OH)$_2$@NF retains 88.3 % of its initial value after a constant operation approximately 100 h at 10 mA cm^{-2},

which signifies the robust stability. Besides, the catalytic activity of Ru/Co$_3$B–Co(OH)$_2$@NF just slightly decays after 1000 cycles (Inset of Figure 6f). Additionally, the SEM characterizations of the catalyst after the HER durability test show that the catalyst surface became rougher (Figure S10c). The excellent durability of Ru/Co$_3$B–Co(OH)$_2$@NF is attributed to the nickel foam self-supporting structure and the strong synergistic effects between Ru and Co$_3$B–Co(OH)$_2$ species.[44]

The Ru/Co$_3$B–Co(OH)$_2$@NF demonstrates excellent catalytic performance on NaBH$_4$ hydrolysis and electrocatalytic hydrogen evolution, where the enhanced catalytic performance is defined by the unique structure and the synergistic effect of Ru clusters, hydrophilic Co(OH)$_2$ species, and conductive metallic Co$_3$B component.[45] XPS analysis confirmed partial electron transfer from Co(OH)$_2$ to Ru clusters, consistent with partial charge transfer due to the different work functions of Ru (4.71 eV) and Co(OH)$_2$ (3.3 eV).[27,46] Therefore, the surface of the Co(OH)$_2$ component is partially positively charged, while the Ru nano-clusters are partially negatively charged. Given the current situation, Langmuir–Hinshelwood mechanism can better corroborate the process of catalyzing the hydrolysis of sodium borohydride.[47] The hydrolysis starts with the adsorption of BH$_4^-$ and H$_2$O over Ru and Co(OH)$_2$, respectively. Then, one of the protonic H of H$_2$O interacts with one of the hydridic H of BH$_4^-$ to liberate one molecule of H$_2$ and the resulting OH$^-$ combines with adsorbed BH$_3$ to form a BH$_3$OH$^-$ intermediate. After that, BH$_3$(OH)$^-$ remains adsorbed and interacts with another H$_2$O molecule to form BH$_2$(OH)$_2^-$ and the second H$_2$ evolves. The process recurs until the fourth H$_2$ evolves. Finally, B(OH)$_4^-$ desorbs.[48] Dramatically, Ru/Co$_3$B–Co(OH)$_2$@NF can also act as an efficient electrocatalyst for an alkaline hydrogen

Chem. Eur. J. **2023**, 29, e202203207 (6 of 8)
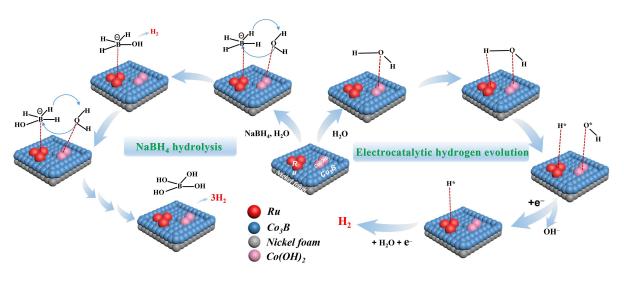
© 2022 Wiley-VCH GmbH

Figure 7. Proposed catalytic mechanism schematics of Ru/Co$_3$B–Co(OH)$_2$@NF catalyst for NaBH$_4$ hydrolysis and electrocatalytic hydrogen evolution.

evolution reaction. The Co(OH)$_2$ can adsorb H$_2$O molecules synergistically and promote the dissociation of H$_2$O to form adsorbed intermediate H* and OH* on Ru and Co(OH)$_2$ interface, respectively. The electronic interaction between Co(OH)$_2$ to Ru and the conductor Co$_3$B facilitates the electron transfer from Co(OH)$_2$ to Ru, which enables the adsorption and dissociation of active intermediates at the interface. The formed H* combines with another electron and H$_2$O molecule, simultaneously releasing H$_2$ and fresh active site for the next cycle (Figure 7).[49]

Conclusion

In summary, we have successfully employed nickel foam as a substrate, combined with electroless plating, low-temperature calcination and impregnation to anchor Ru/Co$_3$B–Co(OH)$_2$ on a 3D structure. The crystal structures and morphologies were characterized by XRD and SEM. Ru clusters were uniformly distributed on the surface of Co$_3$B–Co(OH)$_2$ with an average size of ca. 2.14 nm. XPS spectroscopy revealed substantial charge transfer between Ru and Co(OH)$_2$. Ru/Co$_3$B–Co(OH)$_2$@NF exhibited excellent performance in catalyzing sodium borohydride hydrolysis to hydrogen production with an HGR of 4839.0 mL min^{-1} g^{-1}, which is higher than most of the previously reported catalysts. In addition, the Ru/Co$_3$B–Co(OH)$_2$@NF material demonstrated beyond HER activity with low overpotential (153 mV) to reach 100 mA cm^{-2}, small Tafel slope (40 mV dec^{-1}), high double-layer capacitance (84.9 mF cm^{-2}), and slight charge transfer resistance. Last but not least, the catalyst showed excellent reusability and long-term stability, presenting a potential commercial application.

Conflict of Interest

The authors declare no conflict of interest.

Data Availability Statement

Research data are not shared.

[1] a) S. Q. Wang, B. L. Xu, W. Y. Huo, H. C. Feng, X. F. Zhou, F. Fang, Z. H. Xie, J. K. Shang, J. Q. Jiang, *Appl. Catal. B* **2022**, *313*, 0926–3373; b) J. Zhang, F. Lin, L. Yang, H. Dong, *Chin. Chem. Lett.* **2020**, *31*, 2512–2515.

[2] W. H. Luo, Y. Wang, L. X. Luo, S. Gong, M. N. Wei, Y. X. Li, X. P. Gan, Y. Y. Zhao, Z. H. Zhu, Z. Li, *ACS Catal.* **2022**, *12*, 1167–1179.

[3] J. Y. Guo, B. Z. Wang, D. D. Yang, Z. X. Wan, P. X. Yan, J. N. Tian, T. T. Isimjan, X. L. Yang, *Appl. Catal. B* **2020**, *265*, 118584.

[4] B. W. Jiang, T. Yang, T. T. Wang, C. Chen, M. Yang, X. Y. Yang, J. Zhang, Z. K. Kou, *Chem. Eng. J.* **2022**, *442*, 136119.

[5] H. J. Shen, S. Q. Liang, S. Adimi, X. Y. Guo, Y. Zhu, H. C. Guo, T. Thomas, J. P. Attfield, M. H. Yang, *J. Mater. Chem. A* **2021**, *9*, 19669–19674.

[6] S. Dou, C. Hu, L. Shi, W. Zhang, S. Zhou, P. Yan, L. D'Souza, T. T. Isimjan, X. Yang, *ChemCatChem* **2021**, *13*, 3628–3635.

[7] S. J. Zhao, S. S. Xu, J. L. Yao, N. Chen, Y. T. Gong, X. P. Zhang, X. F. Hao, L. J. Zhang, C. Y. Pei, R. F. Tian, L. L. Wu, B. A. Wan, W. F. Peng, B. Gao, Y. P. Qi, F. M. Gao, R. Ahuja, Y. S. Yao, H. Y. Gou, *J. Mater. Chem. A* **2022**, *10*, 1569–1578.

Chemistry–A European Journal

Research Article
doi.org/10.1002/chem.202203207

Chemistry Europe
European Chemical
Societies Publishing

[8] L. Chen, B. Lu, J. Zhang, R. Wu, Y. Guo, *J. Colloid Interface Sci.* **2022**, *623*, 897–904.

[9] J. Zhang, J. Lian, Q. Jiang, G. Wang, *Chem. Eng. J.* **2022**, *439*, 135634.

[10] A. Paksoy, S. F. Kurtoğlu-Öztulum, M. B. Yağcı, Ö. Balcı-Çağıran, *Int. J. Hydrogen Energy* **2022**, *47*, 36898–36913. .

[11] Z. Chen, K. O. Kirlikovali, K. B. Idrees, M. C. Wasson, O. K. Farha, *Chem* **2022**, *8*, 693–716.

[12] E. Pawelczyk, N. Łukasik, I. Wysocka, A. Rogala, J. Gębicki, *Energies* **2022**, *15*, 4964.

[13] M. D. Allendorf, Z. Hulvey, T. Gennett, A. Ahmed, T. Autrey, J. Camp, E. S. Cho, H. Furukawa, M. Haranczyk, M. Head-Gordon, S. Jeong, A. Karkamkar, D. J. Liu, J. R. Long, K. R. Meihaus, I. H. Nayyar, R. Nazarov, D. J. Siegel, V. Stavila, J. J. Urban, S. P. Veccham, B. C. Wood, *Energy Environ. Sci.* **2018**, *11*, 2784–2812.

[14] C. N. Jin, J. Li, K. Y. Zhang, Habibullah, G. H. Xia, C. L. Wu, Y. Wang, W. L. Cen, Y. W. Chen, Y. G. Yan, Y. G. Chen, *Nano Energy* **2022**, *99*, 2211–2855.

[15] Y. Y. Shang, C. Pistidda, C. Milanese, A. Girella, A. Schokel, T. T. Le, A. Hagenah, O. Metz, T. Klassen, M. Dornheim, *Green Chem.* **2022**, *24*, 4153–4163.

[16] D. Alligier, E. Petit, U. B. Demirci, *Int. J. Hydrogen Energy* **2022**, *47*, 23310–23315.

[17] J. Zhang, F. Lin, L. Yang, Z. He, X. Huang, D. Zhang, H. Dong, *Chin. Chem. Lett.* **2020**, *31*, 2019–2022.

[18] Y. S. Wei, M. S. Wang, W. Y. Fu, L. Wei, X. S. Zhao, X. Y. Zhou, M. Ni, H. J. Wang, *J. Alloys Compd.* **2020**, *836*, 155429.

[19] Y. S. Wei, R. Wang, L. Y. Meng, Y. Wang, G. D. Li, S. G. Xin, X. S. Zhao, K. Zhang, *Int. J. Hydrogen Energy* **2017**, *42*, 9945–9951.

[20] Y. P. Qiu, W. Z. Wang, M. H. Chen, Q. Shi, Z. Q. Yang, P. Wang, *J. Mater. Chem. A* **2021**, *9*, 18385–18392.

[21] G. Bozkurt, A. Ozer, A. B. Yurtcan, *Energy* **2019**, *180*, 702–713.

[22] L. Sun, H. Z. Xu, Z. Y. Cheng, D. H. Zheng, Q. N. Zhou, S. K. Yang, J. J. Lin, *Chem. Eng. J.* **2022**, *443*, 1385–8947.

[23] J. Ge, Y. Cui, Y. Cai, J. Qian, L. Liu, F. Meng, F. Wang, *Composites Part B* **2021**, *224*, 109172.

[24] B. K. Barman, B. Sarkar, K. K. Nanda, *Chem. Commun.* **2019**, *55*, 13928–13931.

[25] L. Ho Jin, P. Eun Duck, *Catalysts* **2022**, *12*, 1203.

[26] S. Dou, C. Hu, L. Shi, W. Zhang, S. Zhou, P. Yan, L. D'Souza, T. T. Isimjan, X. Yang, *ChemCatChem* **2021**, *13*, 3628–3635.

[27] S. Zhou, Y. Yang, W. Zhang, X. Rao, P. Yan, T. T. Isimjan, X. Yang, *J. Colloid Interface Sci.* **2021**, *591*, 221–228.

[28] F. J. Escobar-Bedia, M. Lopez-Haro, J. J. Calvino, V. Martin-Diaconescu, L. Simonelli, V. Perez-Dieste, M. J. Sabater, P. Concepción, A. Corma, *ACS Catal.* **2022**, *12*, 4182–4193.

[29] F. Li, J. Li, L. Y. Chen, Y. M. Dong, P. H. Xie, Q. M. Li, *Int. J. Hydrogen Energy* **2020**, *45*, 32145–32156.

[30] H. Hu, B. Long, Y. Jiang, S. Sun, I. Lawan, W. Zhou, M. Zhang, L. Wang, F. Zhang, Z. Yuan, *Chem. Res. Chin. Univ.* **2020**, *36*, 1209–1216.

[31] M. Guo, Z. Huang, Y. Qu, L. Wang, H. Li, T. T. Isimjan, X. Yang, *Appl. Catal. B* **2023**, *320*, 121991.

[32] X. Zheng, J. Yang, Z. Xu, Q. Wang, J. Wu, E. Zhang, S. Dou, W. Sun, D. Wang, Y. Li, *Angew. Chem. Int. Ed.* **2022**, *61*, e202205946.

[33] H. Zhang, L. Zhang, I. A. Rodríguez-Pérez, W. Miao, K. Chen, W. Wang, Y. Li, S. Han, *Appl. Surf. Sci.* **2021**, *540*, 148296.

[34] L. Shi, K. Zhu, Y. Yang, Y. Liu, S. Xu, T. T. Isimjan, X. Yang, *Int. J. Hydrogen Energy* **2022**, *47*, 37840–37849.

[35] a) L. Yao, X. Li, W. Peng, Q. Yao, J. Xia, Z.-H. Lu, *Inorg. Chem. Front.* **2021**, *8*, 1056–1065; b) Q. Yao, K. Yang, X. Hong, X. Chen, Z.-H. Lu, *Catal. Sci. Technol.* **2018**, *8*, 870–877.

[36] W. Ye, H. Zhang, D. Xu, L. Ma, B. Yi, *J. Power Sources* **2007**, *164*, 544–548.

[37] a) C. Y. Li, Y. Y. Shi, Z. C. Zhang, J. Ni, X. Y. Wang, J. X. Lin, B. Y. Lin, L. L. Jiang, *J. Energy Chem.* **2021**, *60*, 403–409; b) Q. Zhou, Z. J. Zhao, Z. H. Yao, Z. Z. Wei, S. T. Huang, F. J. Shao, A. Y. Li, J. G. Wang, *Catal. Sci. Technol.* **2022**, *12*, 1005–1016.

[38] X. Du, Y. Lang, K. Cao, J. Yang, J. Cai, B. Shan, R. Chen, *J. Catal.* **2021**, *396*, 148–156.

[39] Y. Jiangtao, Z. Yan, N. Xueqing, L. Jun, G. Hongtao, *Int. J. Hydrogen Energy* **2022**, *47*, 29622–29635.

[40] B. Jiang, M. Gil-Sepulcre, P. Garrido-Barros, C. Gimbert-Surinach, J. W. Wang, J. Garcia-Anton, P. Nolis, J. Benet-Buchholz, N. Romero, X. Sala, A. Llobet, *Angew. Chem. Int. Ed.* **2022**, *61*, e202209075.

[41] S. Xu, H. Li, J. Lee, N. Clament Sagaya Selvam, B. Kang, J. Y. Lee, P. J. Yoo, *J. Energy Chem.* **2022**, *69*, 185–193.

[42] Z. Luo, Q. Peng, Z. Huang, L. Wang, Y. Yang, J. Dong, T. T. Isimjan, X. Yang, *J. Colloid Interface Sci.* **2022**, *629*, 111–120.

[43] D. K. Perivoliotis, C. Stangel, Y. Sato, K. Suenaga, N. Tagmatarchis, *Small* **2022**, *18*, e2203032.

[44] a) R. Fiorenza, S. Scirè, A. M. Venezia, *Int. J. Energy Res.* **2018**, *42*, 1183–1195; b) F. Yang, J. Ruan, T. Li, Y. Zou, C. Xiang, F. Xu, L. Sun, *J. Alloys Compd.* **2022**, *926*, 166902.

[45] C. B. Wu, J. F. Zhang, J. A. Guo, L. X. Sun, J. Ming, H. L. Dong, Y. C. Zhao, J. N. Tian, X. L. Yang, *ACS Sustainable Chem. Eng.* **2018**, *6*, 7451–7457.

[46] H. Yang, M. Luo, S. Lu, Q. Zhang, Y. Chao, F. Lv, L. Zhu, L. Bai, L. Yang, W. Wang, D. Wei, Y. Liang, L. Gu, H. Chen, S. Guo, *Chem* **2022**, *8*, 2460–2471.

[47] J. Andrieux, U. B. Demirci, P. Miele, *Catal. Today* **2011**, *170*, 13–19.

[48] U. B. Demirci, P. Miele, *C. R. Chim.* **2014**, *17*, 707–716.

[49] L. X. Wang, Z. Y. Huang, H. X. Huang, S. H. Zhong, M. L. Huang, T. T. Isimjan, X. L. Yang, *Electrochim. Acta* **2022**, *404*, 139598.